ACCURATE CRYSTALLITE SIZE DETERMINATION IN POLY-SI/SIO_X PASSIVATING CONTACTS

Tobias Okker[1], Raphael Glatthaar[1], Frank Huster[1], Sven Seren[2], Thomas Pernau[3], Giso Hahn[1], Barbara Terheiden[1]

[1]University of Konstanz, Universitätsstr. 10, 78464 Konstanz, Germany
[2]Schmid Group, Robert-Bosch-Str. 32-36, 72250 Freudenstadt, Germany
[3]Centrotherm international AG, Württemberger Str. 31, 89143 Blaubeuren, Germany

ABSTRACT: In this work the crystallite size of phosphorus doped polycrystalline-silicon ((n)poly-Si) layers for passivating contacts is determined by X-ray diffraction (XRD) measurements and by scanning electron microscope (SEM) imaging, where a novel preparation technique is used to visualize grain boundaries. For XRD evaluation, it is shown that grazing incidence XRD (GIXRD) measurements lead to signal enhancement for thin poly-Si layers (<300 nm) compared to the Bragg-Brentano configuration. In particular, at low incidence angles of GIXRD measurements, peak broadening caused by an enlarged beam footprint makes crystallite size determination more difficult, especially when using only Scherrer's equation. Thus, crystallite size analysis via Scherrer equation is compared to a Rietveld refinement procedure using a fundamental parameter approach considering instrument and strain broadening, yielding different results. The novel HF-SEM method confirms results obtained through the Rietveld refinement. Key differences in crystallite shape are visible when comparing poly-Si deposited by plasma enhanced chemical vapor deposition (PECVD) and by atmospheric pressure chemical vapor deposition (APCVD), whereas for both techniques the crystallite height agrees well with XRD crystallite size. Comparing both deposition techniques, the crystallite height for APCVD is comparable to the layer thickness, which is different compared to PECVD.

Keywords: poly-Si crystallite size, XRD, SEM

1 INTRODUCTION

With the increasing interest and drive for industrial implementation of TOPCon solar cell concepts in recent years, it is of utmost importance to control the properties of these contacts [1,2]. The doped poly-Si layer exhibits the main impact on the quality of the passivating contact junction, which is located on a thin interfacial SiO_x layer [3]. The poly-Si crystallite size is one of the most important properties of the layer, since it influences the conductivity [4,5] and also the dopant activation and thus the passivation of the junction [6]. In numerous investigations the crystallite size was determined predominantly by XRD, but also by transmission electron microscopy (TEM), and Raman measurements [8-10]. XRD has proven itself as a reliable technique to determine crystallite sizes for which there are two prevalent measurement modes used. The first is the Bragg-Brentano method (here referred to as 2θ-ω mode), where the incidence and detector angle are varied simultaneously [11,12]. This is used for a lot of different applications due to the high-resolution and high intensity without monochromatization or parallelization. The second method is called gracing-incidence-XRD (GIXRD), where a constant low incidence angle is used which is often used to investigate thin films to allow for an increased interaction volume of the X-ray and the poly-Si [13]. Besides the measurement modes, the evaluation of the measurements usually is of higher importance when it comes to the determination of the crystallite size D. This is often done directly via the Scherrer equation for an individual peak at the diffraction angle Θ with

$$D = \frac{K\lambda}{\beta \cos\theta},$$

where K is a factor related to the shape of the crystallites, λ the X-ray wavelength, and β the width of the diffraction peak [14]. However, this neglects additional peak broadening effects from the instrument itself, the strain within the layer, different crystallite size distributions, and other broadening effects [4]. An evaluation that considers all these factors is the Rietveld refinement [15] which is compared to the Scherrer equation approach in this work. As mentioned before, TEM images are also commonly used to determine the poly-Si crystallite size, where additionally the distribution of crystallite sizes can be extracted. In contrast, XRD measurements do not allow accurate conclusions on the size distributions [16]. However, TEM requires time-intensive sample preparation and it is not feasible for large numbers of samples. The other possible imaging microscopy method is scanning electron microscopy (SEM). However, with standard examination of the sample's cross-section, the spatial and in particular the contrast resolution is too small for the grain boundaries of the poly-Si crystallites. Here, we present a preparation method in which the grain boundaries are etched and thus made visible after ion milling of the sample cross-section. In addition, we compare with this method PECVD and APCVD poly-Si regarding crystallite size.

2 EXPERIMENTAL

2.1 Processing

For this work, 150 µm thick n-type Cz-Si wafers with a base doping of 5 Ωcm were saw damage etched with KOH and cleaned in an ozone and piranha solution. Afterwards a 1.7 nm thick thermal oxide was grown in a tube furnace. This was followed by a single sided deposition of phosphorous doped amorphous silicon (a-Si) using an APCVD tool from SCHMID. Multiple drive throughs between 1 and 5 were applied, where each individual layer shows a nominal thickness of 50 nm. Additionally, a PECVD tool by Centrotherm was used to deposit a 140 nm thick (n)a-Si layer on top of the oxide. After that the silicon layers were crystallized in a diffusion furnace at 920°C for 30 min in N_2 atmosphere. Preparation for SEM imaging was done via ion-milling for a few minutes, followed by an HF dip in 2.5% diluted hydrofluoric acid (HF) for 1 s. The HF step presumably

starts to etch the crystallite boundaries at a higher speed than the poly-Si crystallites themselves, increasing the imaging contrast between grain and grain boundary. Crystallite sizes then were determined by investigating multiple images and extracting the crystallite dimensions (length, height and area) by a conventional image editing tool.

2.2 XRD measurements

XRD measurements were conducted using a Bruker D8 Advance in a 2θ range of 20°-70°, using a step width of 0.005°. An exemplary measurement is shown in Fig. 1. A primary divergence slit of 0.2 mm and a 2.5° axial Soller slit was used on the detector side.

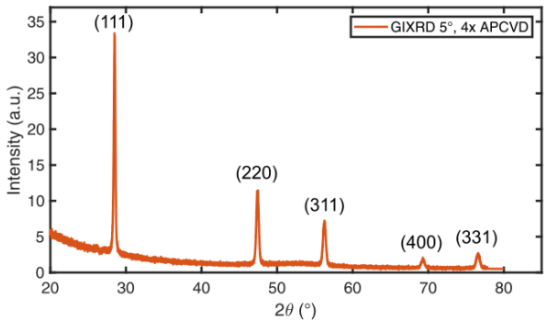

Figure 1: XRD exemplary measurement of a poly-Si layer consisting of 4 drive throughs in the APCVD the corresponding poly-Si peaks are marked.

For usage of the Scherrer equation for determination of the crystallite size, the DIFFRAC.EVA software by Bruker was used to analyze the (111) peak at 2θ=28.5°. Importantly, the integral breadth was used as a measure of the peak width instead of the often-used full width at half maximum (FWHM) which can overestimate the crystallite size [4]. For Rietveld refinement the commercial software Topas was used [17]. The instrumental contribution was modelled via the fundamental parameter approach (FPA) [18], instead of using a reference sample. The refinement includes a polynomial background subtraction, accounting for surface roughness after Pitschke et al. [19] and a zero-error peak shift. Starting with Fd-3m:2 crystal structure, lattice constant, scale factor, and crystallite size were refined. The profile was fitted with a pseudo-Voigt function, whereas for the crystallite size only the Lorentzian part was employed. The fit accuracy was evaluated with R-factors to ensure a comparability between measurements. For a detailed description of the R-factors we refer to [15] or [11]. Furthermore, strain is often not considered when evaluating crystallite size. To quickly estimate the magnitude of strain, Williamson-Hall plots can be used, where strain broadening $\beta_{\mathrm{strain}} = \epsilon \sin\theta$ and crystallite size broadening $\beta_{\mathrm{crystal}} = \frac{K\lambda}{D\cos\theta}$ are added to obtain the measured peak width [20,21]

$\beta_{\mathrm{tot}} = \beta_{\mathrm{strain}} + \beta_{\mathrm{crystal}} \rightarrow \beta_{\mathrm{tot}} \cos(\theta) = \epsilon \sin(\theta) + \frac{K\lambda}{D}$.

This uses the fact that strain and crystallite size have different angular dependencies. To obtain the strain one can graphically solve this equation for strain and crystallite size, as is shown in Fig. 2. This is only a rough estimation, as there are only at maximum 5 poly-Si peaks available for graphical determination. Williamson-Hall-plots show that strain cannot be neglected and are thus considered through a Gaussian contribution in the Topas analysis [13]. Possible sources of strain within the poly-Si are the doping concentration, as it was found that a higher phosphorous concentration can increase strain [22, 23]. Furthermore, annealing and the cooling down step can induce additional stress in the layer [24].

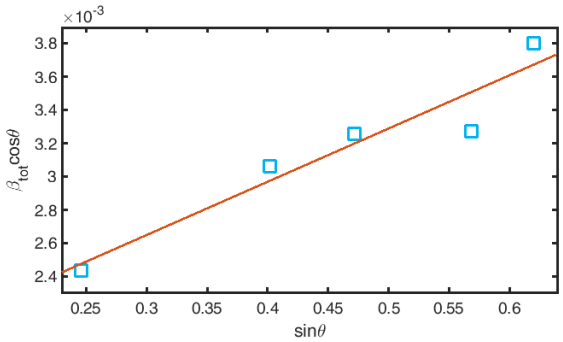

Figure 2: Williamson-Hall plot for the in Fig. 1 shown measurement, yielding an estimation for the crystallite size of D≈78 nm and ε≈0.007.

3 RESULTS

3.1 XRD – Measurement modes

In Fig. 3 XRD profiles of a sample with 5 drive throughs (DT) in the APCVD tool are shown for different measurement modes at the (111) peak. As all measurements were taken with the same detection parameters, one can clearly see that the signal strength is enhanced for the GIXRD measurements which allows for a decreased measurement time compared to the 2θ-ω mode. This is true for all investigated layers with thicknesses <250 nm and is a big advantage of the method as the illuminated sample volume is increased. Especially for even thinner layers (<100 nm), the 2θ-ω mode is more and more unsuitable due to the lacking signal height. Moreover, XRD peaks stemming from the Cz-Si wafer background can interfere with the poly-Si signal in the 2θ-ω mode which is the case for the (400) peak at 70°. However, more importantly it is clearly visible that for a lower incidence angle such as for 1° the XRD peaks broaden immensely due to the beam footprint on to the sample [13]. We found that this broadening is magnified by a larger divergence slit. There have been attempts to consider the beam footprint broadening $G_{hkl}(\omega)$ in Rietveld refinements, as it can be calculated as $G_{hkl}(\omega) = \frac{180}{\pi}\frac{f\sin(2\theta-\omega)}{R\sin(\omega)}$ with the primary slit width f and goniometer radius R [13,25]. This leads to $G_{111}(1°) = 1.94$ and $G_{111}(5°) = 0.37$ and shows the drastic broadening at lower angles. As the peak width is the way to determine the crystallite size from XRD measurements, this broadening presents a hinderance. This broadening is not accounted for in the Topas analysis. Thus, it is not possible to determine the crystallite size for GIXRD 1° measurements via Rietveld refinement with the current Bruker setup available at University of Konstanz. By using a small divergence slit we minimized the broadening effect for GIXRD 5° measurements leading to almost negligible beam footprints. It was found for the samples used here that GIXRD measurements at 5° lead to less peak broadening and thus present a good compromise between signal strength and peak broadening.

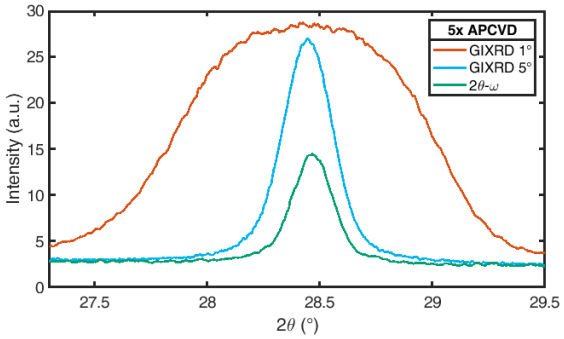

Figure 3: Different XRD measurement modes of the 250 nm thick poly-Si layer accomplished by driving five times through the APCVD System.

3.2 XRD – Analysis of poly-Si layers

The crystallite size stemming from different evaluations and measurement modes for APCVD and PECVD poly-Si are shown in Fig. 4. It is apparent that GIXRD measurements at 1° lead to a rather small crystallite size due to the peak broadening through the beam footprint using the Scherrer equation. On the other hand, GIXRD at 5° produces larger values for crystallite size, while the 2θ-ω mode yields marginally larger crystallite sizes. This points to the fact that, as discussed above, there is still a small peak broadening effect due to beam divergence remaining for most of the samples investigated in this study. However, it has to be pointed out that for the 2θ-ω mode, the signal strength of the 50 nm thick poly-Si layer is reduced immensely compared to GIXRD measurements and requires a longer measurement time to produce valid diffraction peaks. The largest crystallite sizes are obtained from the Rietveld refinement using the FPA approach. Here, the GIXRD and 2θ-ω modes largely agree with one another, leading to crystallite sizes between 50-60 nm. Of course, this crystallite size corresponds to the layers scattering perpendicular to the surface. This is important to keep in mind, as the crystallite shape and distribution is not easily obtainable through XRD measurements.

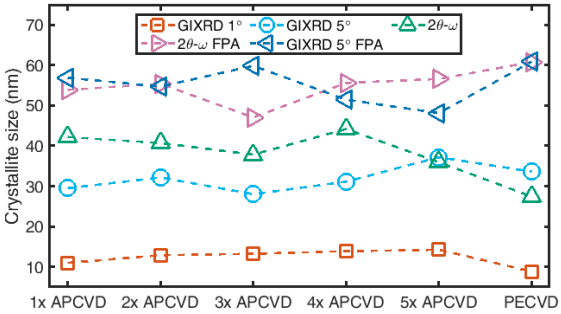

Figure 4: Crystallite sizes for different measurement modes obtained by applying the Scherrer equation and Rietveld Refinement using FPA.

3.3 HF-SEM method

To gain more information about the specific crystallite size distribution within the poly-Si layers and to compare the different evaluation methods, imaging techniques are considered next. For one of the here used APCVD layers, TEM investigations were made. In [26] the poly-Si/SiO_x structure was analyzed on an atomic scale, allowing the resolution of individual crystallites. Moreover, the crystallite height is strongly correlated to the layer thickness. In Fig. 5 SEM images are shown after sample preparation for a 4 DT APCVD layer. As already pointed out in [26], for APCVD the crystallites show a cuboidal shape which are usually wider than high. Furthermore, one striking difference is observable when comparing APCVD and PECVD layers in Fig. 5. Additionally, the crystallite height is limited by the thickness of the individual drive-through layers itself. On the contrary, PECVD poly-Si layers have a less ordered structure, where the crystallites are ordered in no discernible way.

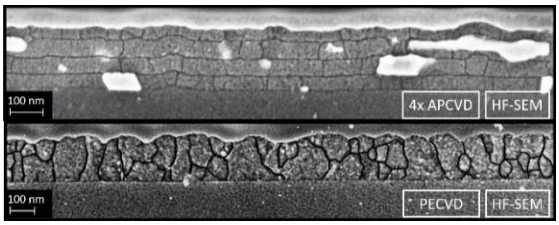

Figure 5: SEM images after preparation with ion-milling and HF for a (top) 4 DT APCVD stack and a (bottom) PECVD layer.

Imaging techniques also allow for determination of a size distribution, as is shown in Fig. 6 where a PECVD and a 5 DT APCVD sample are compared. To obtain the histogram, the crystallite height is shown in Fig. 6. While the distribution is quite narrow around the layer thickness for the APCVD layer, for PECVD layers there is a much wider distribution of crystallite heights which agrees with the expectation from the images in Fig. 5.

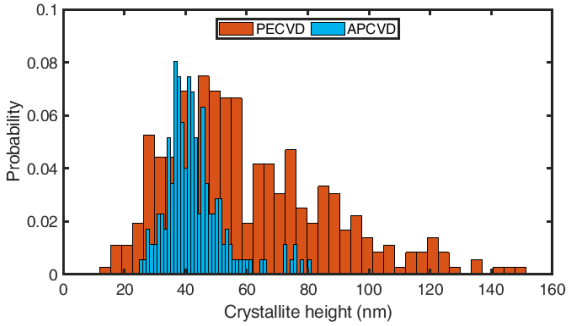

Figure 6: Histogram of a 5 DT APCVD and a PECVD layer, where the occurrence of a respective crystallite height is shown.

Comparing the HF-SEM method with the XRD results in Fig. 7 for the Rietveld refinement, one can see that they largely agree with each other. Of course, neither method is without errors when determining crystallite size. For XRD minimizing the R-factors ensures comparability between the measurements. However, XRD crystallite size mostly presents an estimate which is why no error could be determined. In the case of SEM analysis there are error sources originating from the determination process by hand. These can be related to the resolution of the SEM images as this may be a limiting factor. For some crystallites the boundaries itself also are not able to clearly be identified due to lacking contrast. By averaging multiple images this error can be reduced, but cannot be avoided completely. This should be kept in mind when looking at data from SEM images.

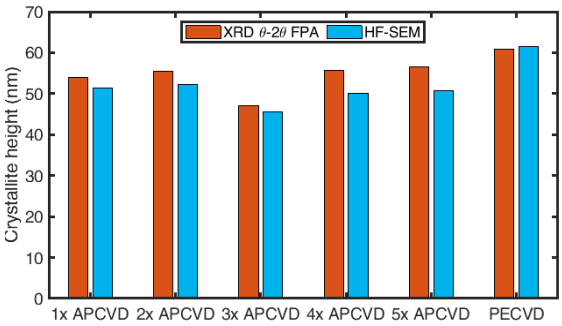

Figure 7: Comparison of XRD crystallite size with the results obtained through analysis of HF-SEM images for APCVD and PECVD layers.

4 CONCLUSIONS

We showed the influence of GIXRD and 2θ-ω measurements on the peak profiles of crystallized APCVD and PECVD (n)poly-Si layers. The peak broadening effects at lower incidence angles can lead to a miscalculation in the crystallite size determination.

Furthermore, a comparison between Scherrer equation and Rietveld refinement using the fundamental parameter approach was made that showed a larger crystallite size for the Rietveld refinement procedure and thus a more reasonable value.

The newly developed HF-SEM method was applied for PECVD and APCVD poly-Si layers and provided results comparable to those of TEM images. This technique revealed the different shape and order of crystallites between APCVD and PECVD poly-Si which was visible in crystallite height distributions.

When comparing HF-SEM and XRD results we found that they agree with each other in the case of an evaluation using Rietveld refinements.

5 AKNOWLEDGEMENTS

Part of this work was financially supported by the German Federal Ministry for Economic Affairs and Climate Action (FKZ 03EE1106B).

6 REFERENCES

[1] D.K. Ghosh, S. Bose, G. Das, S. Acharyya, A. Nandi, S. Mukhopadhyay, A. Sengupta, Surfaces and Interfaces 30 (2022) 101917.
[2] S.W. Glunz, B. Steinhauser, J.-I. Polzin, C. Luderer, B. Grübel, T. Niewelt, A.M.O.M. Okasha, M. Bories, H. Nagel, K. Krieg, F. Feldmann, A. Richter, M. Bivour, M. Hermle, Progress in Photovoltaics: Research and Applications 31 (2021) 341.
[3] T.G. Allen, J. Bullock, X. Yang, A. Javey, S.D. Wolf, Nature Energy 4 (2019) 914.
[4] C. Weidenthaler, Nanoscale 3 (2011) 792.
[5] T. Okker, R. Glatthaar, S. Seren, G. Hahn, B. Terheiden, AIP Conference Proceedings 2826 (2023), 020005.
[6] J.Y.W. Seto, Journal of Applied Physics 46 (1975) 5247.
[7] P.F. Chou, in 2012 IEEE International Reliability Physics Symposium (IRPS), 2012.
[8] J.P. Colinge, E. Demoulin, F. Delannay, M. Lobet, J.M. Temerson, Journal of The Electrochemical Society 128 (1981) 2009.
[9] K. Juraić, D. Gracin, I. Djerdj, A. Lausi, M. Čeh, D. Balzar, Nuclear Instruments and Methods in Physics Research Section B: Beam Interactions with Materials and Atoms 284 (2012) 78.
[10] J.M. Westra, V. Vavruňková, P. Šutta, R.A.C.M.M. van Swaaij, M. Zeman, Energy Procedia 2 (2010) 235.
[11] J. Epp, in Materials Characterization Using Nondestructive Evaluation (NDE) Methods, Elsevier, 2016, 81.
[12] J. Narvaez-Monroy, E. Villalobos-Portillo, L. Fuentes-Cobas, L. Fuentes-Montero, Journal of Physics: Conference Series 1723 (2021) 012047.
[13] D. Simeone, G. Baldinozzi, D. Gosset, S.L. Caer, J.-F. Bérar, Thin Solid Films 530 (2013) 9.
[14] J.I. Langford, A.J.C. Wilson, Journal of Applied Crystallography 11 (1978) 102.
[15] R.E. Dinnebier, A. Leineweber, J.S.O. Evans, Rietveld Refinement, De Gruyter, 2018.
[16] B.B. He, Powder Diffraction 37 (2022) 76.
[17] A.A. Coelho, J. Evans, I. Evans, A. Kern, S. Parsons, Powder Diffraction 26 (2011) 22.
[18] A.L. Ortiz, F.L. Cumbrera, F. Sánchez-Bajo, F. Guiberteau, R. Caruso, Journal of the European Ceramic Society 20 (2000) 1845.
[19] W. Pitschke, H. Hermann, N. Mattern, Powder Diffraction 8 (1993) 74.
[20] D. Nath, F. Singh, R. Das, Materials Chemistry and Physics 239 (2020) 122021.
[21] A.K. Zak, W.H.A. Majid, M.E. Abrishami, R. Yousefi, Solid State Sciences 13 (2011) 251.
[22] C.S. Lee, J.H. Lee, C.A. Choi, K. No, D.M. Wee, Journal of Micromechanics and Microengineering 9 (1999) 252.
[23] K.D. Weeks, S.G. Thomas, P. Dholabhai, J. Adams, Thin Solid Films 520 (2012) 3158.
[24] L. Tutsch, F. Feldmann, B. Macco, M. Bivour, E. Kessels, M. Hermle, IEEE Journal of Photovoltaics 10 (2020) 986.
[25] G. Abbondanza, A. Larsson, F. Carlá, E. Lundgren, G.S. Harlow, Journal of Applied Crystallography 54 (2021) 1140.
[26] R. Glatthaar, F.-P. Schmidt, A. Hammud, T. Lunkenbein, T. Okker, F. Huster, S. Seren, B.C. Greven, G. Hahn, B. Terheiden, Solar RRL (2023).